Enhancing the nonlinear response of plasmonic nanowire antennas by engineering their terminations

Shakeeb Bin Hasan*, Christoph Etrich, Robert Filter, Carsten Rockstuhl, and Falk Lederer

Institute of Condensed Matter Theory and Solid State Optics,

Abbe Center of Photonics, Friedrich-Schiller-Universität Jena,

Max-Wien-Platz 1, 07743 Jena, Germany

Abstract

Sub-wavelength light concentration by means of plasmonic nanoantennas is known to significantly enhance the nonlinear response. In nonlinear schemes involving multiple frequencies, however, it remains challenging to design nanoantennas that respond resonantly to more than one or eventually to all interacting frequencies. Considering plasmonic nanowire antennas, we hereby demonstrate the potential to engineer their resonances at more than one frequencies involved in the nonlinear process by carefully tailoring the antenna terminations. Although we consider here the degenerate nonlinear process of second harmonic generation, our approach can easily be extended to other nonlinear processes.

PACS numbers: 73.20.Mf, 42.65.Ky, 42.65.Wi

I. INTRODUCTION

In recent years, plasmonics has established itself as a promising route towards the nano-scale miniaturization of optical elements[1]. The physical principle which plasmonics is based on is the coupling of electromagnetic radiation to the oscillation of the charge density in noble metals at the metal-dielectric interface[2]. The interest in plasmonics has spurred an ever-growing research as well as a body of literature reporting the observation of various optical phenomena in such systems which could be of use in integrated optics and spectroscopic applications, among others. The sub-wavelength confinement of light leads to a minimization of the geometrical scale where linear effects are observed, which yields a stronger nonlinear interaction due to the high field intensities available in the near field[3]. This triggered investigations into understanding the extent to which strong field localization can beneficially affect the nonlinear process in the face of resistive losses present in metals (for instance, see[4–9]).

In general, it can be distinguished between the intrinsic and extrinsic nonlinear properties of nanooptical systems[10]. The intrinsic nonlinearity refers to systems where the metals themselves are the sole source of a nonlinear polarization. This makes it possible, for example, to observe a strong third-order nonlinear response. This allows to generate, e.g., a third harmonic signal upon excitation of optical nanoantennas[11,12]. Alternatively, at the surface of the optical nanoantenna the mirror-symmetry of the lattice might be broken and second-order nonlinear effects can be encountered[13,14]. This equally holds while discussing the properties of metals beyond the ordinary Drude model, e.g., semi-classical hydrodynamic model to describe the dynamics of the free electrons[15–18] or considering quantum-tunneling effects if two plasmonic elements are brought sufficiently close such that electron coupling across the gap results in extreme non-locality[19–21]. Another interesting mechanism of SH generation in centrosymmetric media is the Lorentzian interaction of electric and magnetic field components of the modes[22]. On the contrary, much work was done also studying optical nanosystems with an extrinsic nonlinearity[23,24]. The optical nanoantenna's role is to localize light into large near field intensities which causes an enhanced nonlinear response from the surrounding nonlinear dielectric medium. Such a case is considered here without any loss of generality.

As a general rule, the nonlinear processes involve the interaction of light oscillating at multiple frequencies depending on the order of nonlinearity and the specific nature of interaction under consideration. This makes it ideal, if not necessary, to have plasmonic elements that are resonant to all the frequencies involved. Recent studies have attempted to conceive such nanostructures by employing innovative antenna designs that afford tunability at multiple frequencies[22,25–30]. Some of these approaches choose a path were a few individual nanoantennas that sustain resonances at selected frequencies are fused into a single structure. This assures the requirement of having a nanoantenna that sustains resonances at all frequencies of interest[26–28]. In other approach, the geometrical features of a composite nano-particle, whether isolated or in array, are tailored to achieve the same end by employing orthogonal polarizations for interacting frequencies[22,25]. In both cases, however, it is challenging to achieve a good spatial overlap - necessary for strong nonlinear response - among the modes at different frequencies which might localize in different arms of the composite antenna geometry. Additionally, the second approach also requires the interacting frequencies to be orthogonally polarized. This can also be a potential drawback when considering the commonly employed quadratic media exhibit their strongest response through d_{33} component of their polarizability tensor which is best utilized if the interacting frequencies are polarized in the same direction. Moreover, it is easy to realize that the fabrication of such structures that consist of multiple elements remains a challenge for current nano-fabrication. Even though many top-down as well as bottom-up approaches for nano-fabrication are developed, the precise alignment of the individual elements to form the actual nanoantenna constitutes an unnecessary complication. Therefore, it is desirable to have available compact and isolated nanoantennas that can sustain resonances at frequencies on demand.

It is the aim of this paper to explore the potential of cylindrical nanowires as an ideal platform to tailor the nonlinear interaction of light with matter and which meets both aforementioned requirements. Most notably, we will show here that with only a single structural entity it is possible to devise nanoantennas that sustain resonances at multiple frequencies which are involved in the nonlinear process. These optical nanowire antennas are superior for various reasons when compared to many other nanoantennas. First, their basic functionality is well understood by now, even on the basis of semi-analytical models[31,32]. Second, various fabrication methods have been proven to be applicable to realize those nanoantennas with high precision[33].

Starting point of the approach to our antenna design is the appreciation that it is not just the length of the nano-antenna that dictates the resonance frequency. Equally the termination of the nanoantenna can provide a significant degree of freedom for tailoring the response of the system. In fact, in limiting cases the termination can even account for the localized resonances exhibited by analytically understood nanoparticles in the quasi-static limit[34]. In these optical nanoantennas a resonance is supported whenever the phase accumulation of a surface plasmon polariton that bounces back and forth in the nanowire experiences a phase accumulation of a multiple of 2π. Contributions to this phase accumulation are due to the propagation along the nanowire, i.e., determined by the dispersion relation, but also by the phase of the complex reflection coefficient. It is essential to stress that both quantities may have a tailored dispersion that can be independently controlled to a large extent. Designing and engineering the nanoantenna termination with the purpose to tailor the antenna resonances is an often underestimated opportunity. Thus it is only natural to consider the antenna terminations towards an enhancement of multi-frequency nonlinear processes as discussed above.

To this end, we combine in our contribution a multitude of theoretical and numerical means to explore the opportunities to tailor the second-order nonlinear response of nanowire antennas embedded in lithium niobate ($LiNbO_3$). Specifically, we utilize an analytical model that can precisely predict the resonances, use a coupled-field theory approach to calculate the strength of the nonlinear response, and verify all our predictions using full-wave simulations that take into account the nonlinear process correctly.

II. LINEAR PROPERTIES

Figure 1(a) sketches the antenna geometry under consideration. It consists of a cylindrical nanowire of length L that has a semi-ellipsoidal cap as termination. Two of the three semi-axes of the cap perpendicular to cylinder's axis are equal to the radius of the nanowire whereas the third semi-axis a [Fig .1(a)] parallel to cylinder's axis is allowed to be different. This serves as an additional degree of freedom to tailor the response of the nanoantenna. The limiting case of $a = 0$ would make it an abrupt termination whereas the limiting case of $L = 0$ would cause the antenna to collapse towards an ellipsoidal nano-particle[34]. When illuminated with a plane wave whose electric field is polarized along the cylinder's axis (x-axis) and propagating along the z-axis [Fig. 1(a)], a propagating surface plasmon polariton is excited

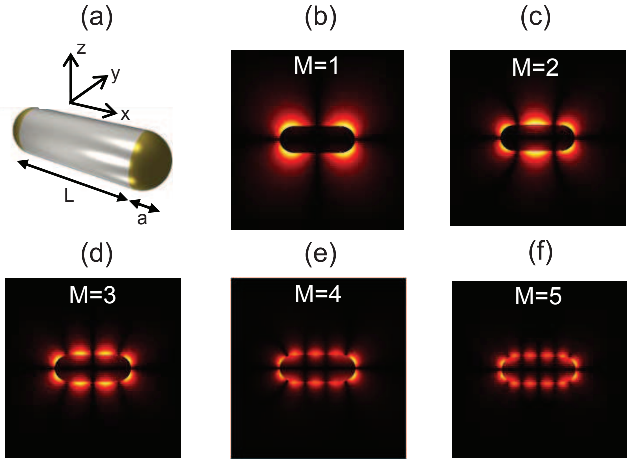

FIG. 1: (a) Cylindrical nanowire of length L terminated by semi-ellipsoidal caps on both sides. Two semi-axes of these caps are shared with the radius of the nanowire whereas the third axis is a free parameter, labeled as a. (b-f) $|E_{\mathrm{y}}|$ distribution of FP modes of order M when the antenna is illuminated by an x-polarized plane wave propagating along z-axis. For exciting modes with even M, the exciting wave was inclined with respect to the z-axis on the $x-z$-plane in order to break the symmetry.

on the nanowire. It bounces back and forth between the semi-ellipsoidal terminations where it causes the nanoantenna to sustain eventually Fabry-Perot (FP) resonances at specific frequencies for a fixed geometry. The requirement to observe an antenna resonance at a frequency ν can be described as[31,33,34]

$$\beta^{'}(\nu)L + \phi_{\mathrm{r}}(a,\nu) = m\pi \tag{1}$$

where $\beta^{'}(\nu) = \Re\{\beta(\nu)\}$ is the real part of the propagation constant, $\phi_{\mathrm{r}}(a,\nu)$ the phase of the modal reflection coefficient $r(a,\nu)$, L the length of the cavity, and m an integer denoting the order of the FP resonance. The reasoning for the antenna resonance derives from the requirement that the phase accumulation per round trip shall be a multiple of 2π. It should be pointed out that only symmetric antennas are considered here, i.e., those where the antenna capping is identical for both terminations. Figures 1(b-f) plot the $|E_{\mathrm{y}}|$ field distribution of FP resonances of various order m in the $x-z$ cross section of the antenna. It should be noted that unlike odd order resonances, even order ones are forbidden by symmetry and were excited by the incoming wave inclined with respect to the z-axis on

$x - z$ plane [Fig. 1(a)] .

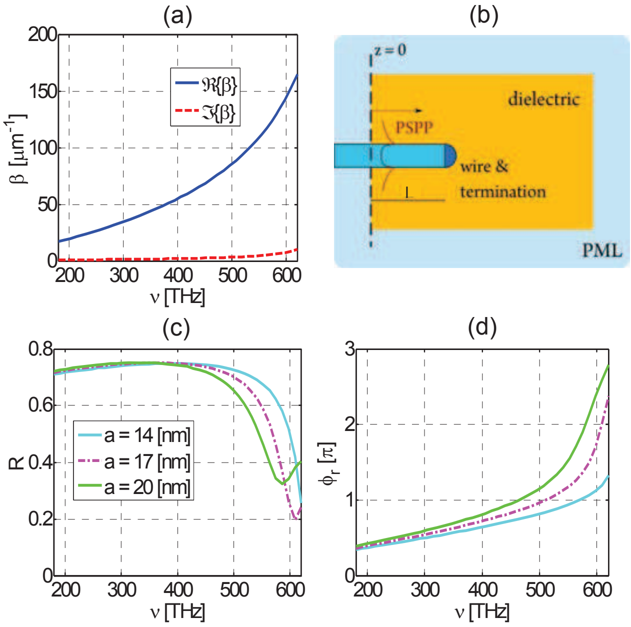

FIG. 2: (a) Dispersion of fundamental TM_0 mode computed for a cylindrical wire of radius 15nm. (b) Schematic illustration of the 3D geometry used for obtaining the modal reflection coefficient $r(a,\nu)$ of TM_0 mode. (c) Squared amplitude $R(a,\nu) = |r(a,\nu)|^2$ (c) and (d) phase $\phi_r(a,\nu) = \arg[r(a,\nu)]$ of the reflection coefficient are also shown.

To numerically model the system, we describe the metallic nanoantenna using a Drude fit of Ag[35] defined by the plasma frequency $\omega_p = 1.88 \times 10^3$THz and damping $\gamma = 19.3$THz. The surrounding dielectric medium is assumed to be $LiNbO_3$ whose dispersion is isotropically defined, for the sake of computational simplicity, through the extraordinary axis by means of a Sellmeir fit[36]. The anisotropy of the nonlinear $\chi^{(2)}$ tensor, however, is fully considered and its c-axis is aligned to the x-axis [Fig. 1(a)] to make the most out of the strongest d_{33} coefficient. Since numerical techniques based on finite element method (FEM) are more suitable to capture geometrical curvature[37], we employed a commercial FEM based electromagnetic solver COMSOL MULTIPHYSICS to compute the linear dispersion of the complex modal propagation constant $\beta(\nu)$ of the fundamental TM_0 mode on a cylindrical nanowire of 15nm radius [Fig .2(a)]. As the radius of the nanowire is sufficiently small compared to the wavelength (quasi-statics), we need not to consider any higher transversal mode supported by the nanowire[31,34]. In order to obtain the modal reflection coefficient from the terminal cap, we employ a computational setup shown in Fig. 2(b). The eigenmode is launched at $z = 0$ plane where the back-reflection from the antenna termination gets absorbed into the perfectly matched layers (PML) surrounding the computational window. A straightforward application of the orthogonality relation established through the unconjugated reciprocity theorem[38] leads to the following equation for the modal reflection coefficient:

$$r(a,\nu) = -\exp(-i2\beta' l)\frac{\int_0^\infty E_{\rho,0}(\rho,\nu)\left[H_\phi(\rho,z=0,a,\nu) - H_{\phi,0}(\rho,\nu)\right]\rho\,\mathrm{d}\rho}{\int_0^\infty E_{\rho,0}(\rho,\nu)H_{\phi,0}(\rho,\nu)\rho\,\mathrm{d}\rho}. \tag{2}$$

The symbols $E_{\rho,0}(\rho,\nu)$ and $H_{\phi,0}(\rho,\nu)$ denote the radially and azimuthally polarized electric and magnetic field components of the eigenmode supported by an infinitely extended nanowire, respectively. Likewise, $H_\phi(\rho,z,a,\nu)$ denotes the total magnetic field within the computational domain that introduces the dependence upon the cap radius a. The length l of the antenna in Fig. 3(b) was chosen large enough as to remove any dependance of $r(a,\nu)$ on it due to coupling to higher order evanescent modes, although the application of orthogonality relations should already have significantly suppressed it. At $z = 0$ plane, $H_\phi(\rho,z=0,a,\nu)$ is a superposition of incident and reflected modes from which the contribution of the incident eigenmode is subtracted to obtain the reflection coefficient. Figures 2(c,d) display the squared amplitude $R = |r(a,\nu)|^2$ and phase $\phi_r(a,\nu) = \arg[r(a,\nu)]$ of the dispersive modal reflection coefficient.

Given the strong dispersion of $r(a,\nu)$ [Fig. 2(c-d)] upon both frequency and cap geometry, we attempt to explore the possibility to align FP resonances of different orders with the frequencies taking part in the nonlinear process. To this end, we propose to exploit the semi-axis a of the cap as a degree of freedom in design parameters while keeping the radius of the nanowire constant. This can be desirable in circumstances where strong field localization is required because the fundamental TM_0 mode shows increasing localization with decreasing wire radius[34]. As for the specific nonlinear interaction considered, we choose to work with the degenerate nonlinear process of second-harmonic generation (SHG) when the metallic cylinder is embedded in a dielectric medium possessing a $\chi^{(2)}$ response. More complex scenarios involving three- or four-wave mixing (cubic media) can be explored along the same lines.

III. NONLINEAR PROPERTIES

¿From the linear simulations we can extract all the information necessary to predict the spectral position of the FP resonances of the antenna. In terms of the antenna length L, the resonance condition of Eq. (1) can be written as

$$\begin{aligned} L_m &= \frac{m\pi - \phi_{\mathrm{r}}(a, \nu_{\mathrm{FH}})}{\beta'(\nu_{\mathrm{FH}})}, \\ L_n &= \frac{n\pi - \phi_{\mathrm{r}}(a, 2\nu_{\mathrm{FH}})}{\beta'(2\nu_{\mathrm{FH}})}, \end{aligned}$$

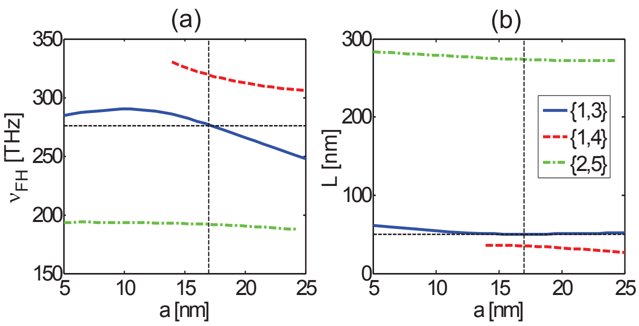

FIG. 3: (a) Pump frequency ν_{FH} and (b) length L for the given cap radius a where double resonance is possible for FP orders m, n at FH and SH respectively. Horizontal and vertical black lines indicate the operating configuration ($\nu = 276$THz, $a = 17$nm and $L = 50$nm) chosen in this study.

where m and n are integers denoting the order of the FP resonances at FH and SH frequencies, respectively. In order to find configurations whith a resonant response at both the fundamental (FH) and corresponding second harmonic (SH), we solve for the condition $L_m = L_n$. Figure 3 displays the result when the semi-axis a is varied from 5nm to 25nm and the FH frequency from 180THz to 320THz. The figures have to be read such that for a desired operation frequency of the FH a certain semi-axis a can be derived [cf. Fig. 3(a)]. Using this specific a the corresponding antenna length L can be read off from Fig. 3(a-b), such that the corresponding antenna sustains a resonance at both the FH and the SH frequencies. Allowing for different FP orders at FH and SH, we obtained doubly-resonant configurations for the combination of 1^{st} order at FH with 3^{rd} and 4^{th} order at SH, and the combination of 2^{nd} order at FH with 5^{th} order at SH, as indicated in the figure. It can be seen that a suitable design that covers the entire frequency spectrum is not found for the present rather restrictive geometry. However, for quite a large spectral domain in multiple intervals double resonant nanoantennas can be perceived.

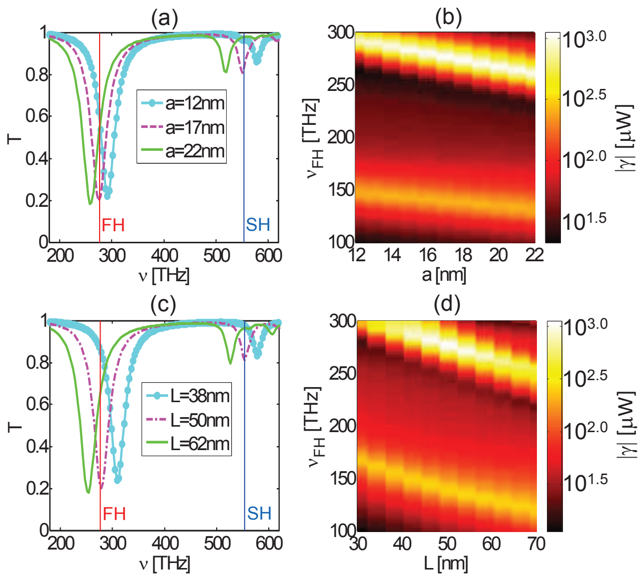

FIG. 4: (a) Linear transmission spectrum and (b) nonlinear mode overlap $|\gamma|$ for cap detuning. Likewise, (c) and (d) show the linear transmission and mode overlap when the length of the antenna is detuned. The nonlinear mode overlap is obtained by illuminating with a pump of power 1W per unit cell. Please note that $|\gamma|$ is shown on a logarithmic scale.

Considering only the bright resonances, i.e. excitable resonances, under normal illumination (parallel to the z-axis [Fig. 1(a)]), we shall exclusively work with the scheme exhibiting 1^{st} and 3^{rd} order resonances at FH and SH frequency, respectively, in Fig. 3. However, this is by no means a general restriction because the other combinations could have been explored as well.

In order to compare the predicted resonance frequencies to those supported by the actual structure, first we performed linear full wave simulations. Specifically, we considered an array of antennas arranged in a periodic lattice of 200nm $\times$ 200nm in the transverse $x - y$ plane. The period was chosen large enough such that the interaction among neighboring nanoantennas may be disregarded. Choosing a test case of a = 17nm, we find L = 50nm and ν_{FH} = 277THz as the configuration for double resonance from Fig. 3. The periodic array is excited with x-polarized light according to Fig. 1(a) to compute the linear response of the system. Figures. 4 (a) and (c) show the transmission results when the cap semi-axis

a and the length L of the antenna are detuned. A detailed inspection clearly demonstrates the double resonance characteristic at both FH and SH in the fully resonant case. It can be extracted from the figure that the resonances predicted with the analytical model are indeed supported by the structure at the correct frequencies.

To theoretically understand the advantage of doubly resonant antennas for nonlinear interaction, in a second step we take advantage of the undepleted pump approximation to describe the nonlinear interaction of the near fields at both the FH and SH frequency[39]. Accordingly, the strength of the nonlinear interaction is described in terms of an effective nonlinear coefficient γ which depends crucially on the field overlap and is defined under Kleinman's symmetry as

$$\gamma \approx \varepsilon_0 \nu_{\mathrm{FH}} \iiint d_{33}(\mathbf{r}) E_{\mathrm{x}}^2(\mathbf{r}, \nu_{\mathrm{FH}}) E_{\mathrm{sx}}^{\star}(\mathbf{r}, 2\nu_{\mathrm{FH}}) d\mathbf{r}, \tag{3}$$

where $E_{\mathrm{x}}(x, y, \nu)$ is the x-component of the total FH field (incident plane wave and scattered field by the periodic array) while $\mathrm{E}_{\mathrm{sx}}(\mathbf{r}, \nu)$ denotes the x-component of the scattered (without excitation at SH frequency) SH field. Equation (3) is approximately written in terms of the dominant d_{33} coefficient of the contracted $\chi^{(2)}$ tensor which is at least one order of magnitude stronger than the rest[36]. In numerical simulations, however, the full anisotropic $\chi^{(2)}$ tensor is taken into account.

By illuminating the periodic array with a plane wave of power 1W per unit cell, we scanned for the variation of $|\gamma|$ in case of cap and length detuning as before. The results are shown in Fig. 4(b,d). We find an enhancement in $|\gamma|$ by approximately twice the order of magnitude when $\nu_{\mathrm{FH}} = 277$THz and the cap axis $a = 17$nm [Fig. 4(b)] or length $L = 50$nm [Fig. 4(b)]. Another bright line is also visible when the incident pump frequency is $\nu_{\mathrm{FH}} = 139$THz. This happens because the corresponding SH frequency coincides with the first order FP resonance of the antenna and the nonlinear response is equally enhanced in such a single-resonant configuration although less pronounced.

To corroborate the predicted enhancement in nonlinear interaction, we performed nonlinear full-wave simulations using our in-house code based on finite-difference time-domain (FDTD) method. The grid size in the discretized space was chosen to be 1nm whereas metallic and dielectric dispersion was incorporated through the fits described earlier. The instantaneous nonlinear response of the dielectric medium was incorporated into the FDTD simulation as[40]:

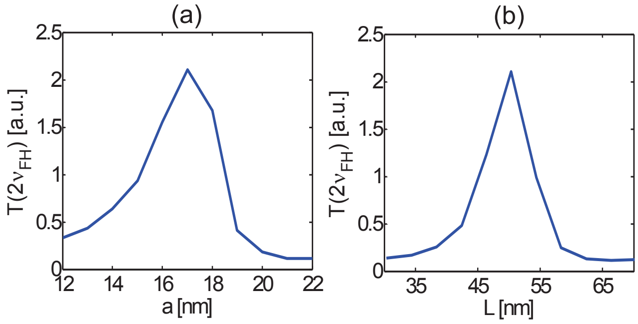

FIG. 5: (a) Transmission spectrum of nonlinear FDTD simulations when illuminated with a CW pump of power 13mW at $\nu = 277$THz showing the effect of detuning the cap radius a where $L = 50$ nm(a) and (b) length L where $a = 17$ nm from their resonant values of $a = 17$nm and $L = 50$nm, respectively.

$$\mathbf{P}^{(2)}(\mathbf{r},t) = 2\varepsilon_0 \begin{pmatrix} d_{33}(\mathbf{r})E_{\mathrm{x}}(\mathbf{r},t)^2 + d_{31}(\mathbf{r})E_{\mathrm{y}}(\mathbf{r},t)^2 \\ 2d_{31}(\mathbf{r})E_{\mathrm{x}}(\mathbf{r},t)E_{\mathrm{y}}(\mathbf{r},t) \\ 0 \end{pmatrix} \tag{4}$$

For the sake computational simplicity, we omitted in our code [hence Eq. (4)] those components of the contracted $\chi^{(2)}$ tensor which introduce dependance on E_{z} field which is negligibly smaller than others. Illuminating the periodic array with a continuous-wave (CW) pump at $\nu_{\mathrm{FH}} = 277$THz and carrying 13mW power per unit cell, we computed the power flux in transmission at SH through a periodic cell. Figures. 5 show the results for the two specific cases of cap and length detuning discussed earlier in parts (a) and (b) respectively. An order of magnitude enhancement is observed in the generated SH when the geometrical parameters coincide with the doubly resonant configuration [Fig. 4(a,c)] clearly demonstrating the advantage of our scheme.

The scenarios discussed so far, however, do not fully distinguish the merit of having doubly resonant antennas. Therefore, we calculated the antenna configuration when illuminated at the same frequency ($\nu_{\mathrm{FH}} = 277$THz) but the geometrical parameters are varied to only keep either of the two resonances at pump or SH frequency as shown in Fig. 6(a). To clarify the role of the resonance at SH, we chose to work on the red line in Fig. 6(a) which describes the geometrical configuration where the antenna is always resonant at $\nu_{\mathrm{FH}} = 277$THz. It can be clearly seen that the SH is only resonant, in general, for a slightly different geometry except

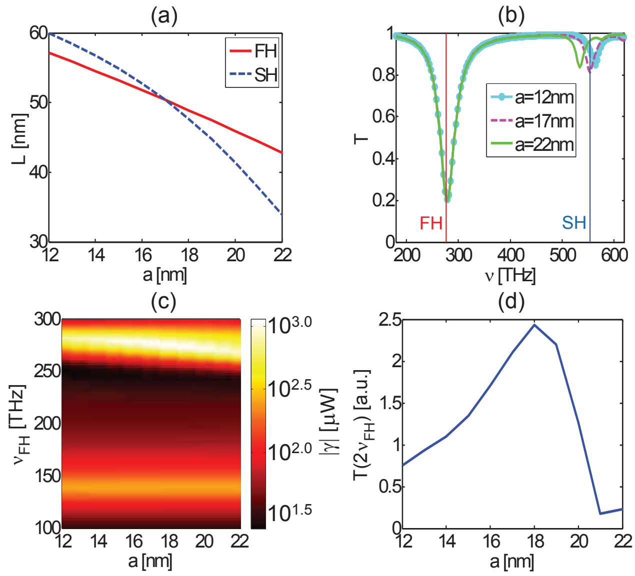

FIG. 6: (a) Antenna configuration at $\nu_{\rm FH} = 277$THz when FH has FP resonance of 1$^{\rm st}$ and SH of 3$^{\rm rd}$ order. (b) Linear transmission spectrum and (c) nonlinear mode overlap $|\gamma|$ are shown when the antenna is kept resonant at FH according to (a). Likewise, the transmission spectrum of nonlinear FDTD-simulations is shown in (d) when the structure is illuminated with a pump of $\nu_{\rm FH} = 277$THz.

for a specific, the doubly resonant configuration. Only if this configuration is met, a double resonant scheme is achieved whereas otherwise the nanoantenna is only single resonant at FH.

Figure. 6(b) shows the corresponding results of linear transmission simulation performed in the same manner as discussed earlier in the context of Fig. 4. We find the FH to be always resonant at $\nu_{\rm FH} = 277$THz as enforced but the SH is detuned except when the cap semi-axis is $a = 17$nm. Figure. 6(c) scans the value of $|\gamma|$. The bright line in Fig. 6(c) at $\nu_{\rm FH} = 139$THz shows no geometrical dependance because the antenna is always resonant at the corresponding SH. But the bright line around $\nu_{\rm FH} = 277$THz is slanted indicating a prominent dependance upon the SH resonance of the antenna which keeps changing for different geometrical configurations. Figure 6(d) shows the computed SH transmission spectrum in nonlinear FDTD-simulations whose computational details are the same as described earlier. The peak for the largest second harmonic signal is reached in Fig. 6(c) for $a = 18$nm which is close enough to the predicted value of $a = 17$nm. This minor deviation can be attributed to disparity between the numerical methods - FEM for the analytical prediction while the FDTD-method was employed for nonlinear computations. However, overall we see an excellent agreement and a clear demonstration of the positive impact doubly resonant antennas can have on enhancing the efficiency of nonlinear interaction.

IV. CONCLUSION

In conclusion, we proposed and numerically demonstrated that a simple plasmonic antenna consisting of a cylindrical metallic nanowire with semi-ellipsoidal terminations provided already sufficient degrees of freedom such that it can be tuned to have double resonance sustained across an extended range of incident frequencies. Through rigorous linear and nonlinear full wave FDTD-simulations, the superiority of doubly resonant structures over singly-resonant ones was demonstrated for the specific case of second-harmonic generation. The key that unlocked these tuning opportunities was the appreciation that the terminations of the nanoantennas, i.e. their cappings, can be independently controlled from the main body of the nanoantenna, i.e. the wire. This degree of freedom was thus far not exploited in the context of nonlinear plasmoncics. Although the fabrication of the suggested structures sound challenging, nowadays available high resolution top dow nano-fabrication techniques, e.g. based on Helium-Ion-Lithography can be used in perspective. Alternatively, bottom-up approaches can also be used, e.g. based on the controlled reduction of a metal salt on an existing nanowire for homogenous material systems[41] but also for heterogenous material systems[42] if desired. Our findings have the potential to greatly enhance the outcome of more complex, nondegenerate parametric interactions leading to novel applications in optical spectroscopy and computing.

Acknowledgements

Support by the German Federal Ministry of Education and Research (PhoNa), by the Thuringian State Government (MeMa), and the German Science Foundation (SPP 1391

Ultrafast Nano-optics) is acknowledged.

[1] D. K. Gramotnev and S. I. Bozhevolnyi, Nat Photon **4**, 83 (2010), ISSN 1749-4885, URL http://dx.doi.org/10.1038/nphoton.2009.282.

[2] S. A. Maier, *Plasmonics: Fundamentals and Applications* (Spri, 2007).

[3] M. Kauranen and A. V. Zayats, Nat Photon **6**, 737 (2012), ISSN 1749-4885, URL http://dx.doi.org/10.1038/nphoton.2012.244.

[4] K. D. Ko, A. Kumar, K. H. Fung, R. Ambekar, G. L. Liu, N. X. Fang, and K. C. Toussaint, Nano Letters **11**, 61 (2011), http://pubs.acs.org/doi/pdf/10.1021/nl102751m, URL http://pubs.acs.org/doi/abs/10.1021/nl102751m.

[5] M. Ren, E. Plum, J. Xu, and N. I. Zheludev, Nat Commun **3**, 833 (2012), URL http://dx.doi.org/10.1038/ncomms1805.

[6] G. Hajisalem, A. Ahmed, Y. Pang, and R. Gordon, Opt. Express **20**, 29923 (2012), URL http://www.opticsexpress.org/abstract.cfm?URI=oe-20-28-29923.

[7] S. Linden, F. B. P. Niesler, J. Förstner, Y. Grynko, T. Meier, and M. Wegener, Phys. Rev. Lett. **109**, 015502 (2012), URL http://link.aps.org/doi/10.1103/PhysRevLett.109.015502.

[8] S. B. Hasan, C. Rockstuhl, T. Pertsch, and F. Lederer, J. Opt. Soc. Am. B **29**, 1606 (2012), URL http://josab.osa.org/abstract.cfm?URI=josab-29-7-1606.

[9] A. R. Davoyan, I. V. Shadrivov, and Y. S. Kivshar, Opt. Express **17**, 21732 (2009), URL http://www.opticsexpress.org/abstract.cfm?URI=oe-17-24-21732.

[10] T. Utikal, T. Zentgraf, T. Paul, C. Rockstuhl, F. Lederer, M. Lippitz, and H. Giessen, Phys. Rev. Lett. **106**, 133901 (2011), URL http://link.aps.org/doi/10.1103/PhysRevLett.106.133901.

[11] J. Reinhold, M. R. Shcherbakov, A. Chipouline, V. I. Panov, C. Helgert, T. Paul, C. Rockstuhl, F. Lederer, E.-B. Kley, A. Tünnermann, et al., Phys. Rev. B **86**, 115401 (2012), URL http://link.aps.org/doi/10.1103/PhysRevB.86.115401.

[12] M. Hentschel, T. Utikal, H. Giessen, and M. Lippitz, Nano Letters **12**, 3778 (2012), http://pubs.acs.org/doi/pdf/10.1021/nl301686x, URL http://pubs.acs.org/doi/abs/10.1021/nl301686x.

[13] A. Slablab, L. L. Xuan, M. Zielinski, Y. de Wilde, V. Jacques, D. Chauvat, and J.-F.

Roch, Opt. Express **20**, 220 (2012), URL http://www.opticsexpress.org/abstract.cfm?URI=oe-20-1-220.

[14] J. Butet, I. Russier-Antoine, C. Jonin, N. Lascoux, E. Benichou, and P.-F. Brevet, J. Opt. Soc. Am. B **29**, 2213 (2012), URL http://josab.osa.org/abstract.cfm?URI=josab-29-8-2213.

[15] C. Ciracì, E. Poutrina, M. Scalora, and D. R. Smith, Phys. Rev. B **86**, 115451 (2012), URL http://link.aps.org/doi/10.1103/PhysRevB.86.115451.

[16] C. Ciracì, E. Poutrina, M. Scalora, and D. R. Smith, Phys. Rev. B **85**, 201403 (2012), URL http://link.aps.org/doi/10.1103/PhysRevB.85.201403.

[17] P. Ginzburg, A. Krasavin, Y. Sonnefraud, A. Murphy, R. J. Pollard, S. A. Maier, and A. V. Zayats, Phys. Rev. B **86**, 085422 (2012), URL http://link.aps.org/doi/10.1103/PhysRevB.86.085422.

[18] T. Paul, C. Rockstuhl, and F. Lederer, Journal of Modern Optics **58**, 438 (2011), http://www.tandfonline.com/doi/pdf/10.1080/09500340.2010.511291, URL http://www.tandfonline.com/doi/abs/10.1080/09500340.2010.511291.

[19] K. J. Savage, M. M. Hawkeye, R. Esteban, A. G. Borisov, J. Aizpurua, and J. J. Baumberg, Nature **491**, 574 (2012), ISSN 0028-0836, URL http://dx.doi.org/10.1038/nature11653.

[20] J. A. Scholl, A. GarcÃa-Etxarri, A. L. Koh, and J. A. Dionne, Nano Letters **13**, 564 (2013), http://pubs.acs.org/doi/pdf/10.1021/nl304078v, URL http://pubs.acs.org/doi/abs/10.1021/nl304078v.

[21] R. Esteban, A. G. Borisov, P. Nordlander, and J. Aizpurua, Nat Commun **3**, 825 (2012), URL http://dx.doi.org/10.1038/ncomms1806.

[22] B. Z. Steinberg, Opt. Express **19**, 25843 (2011), URL http://www.opticsexpress.org/abstract.cfm?URI=oe-19-27-25843.

[23] C. Argyropoulos, P.-Y. Chen, G. D'Aguanno, N. Engheta, and A. Alù, Phys. Rev. B **85**, 045129 (2012), URL http://link.aps.org/doi/10.1103/PhysRevB.85.045129.

[24] P.-Y. Chen and A. Alu, Nano Letters **11**, 5514 (2011), http://pubs.acs.org/doi/pdf/10.1021/nl203354b, URL http://pubs.acs.org/doi/abs/10.1021/nl203354b.

[25] U. K. Chettiar and N. Engheta, Phys. Rev. B **86**, 075405 (2012), URL http://link.aps.org/doi/10.1103/PhysRevB.86.075405.

[26] H. Harutyunyan, G. Volpe, R. Quidant, and L. Novotny, Phys. Rev. Lett. **108**, 217403 (2012),

URL http://link.aps.org/doi/10.1103/PhysRevLett.108.217403.

[27] M. Abb, Y. Wang, P. Albella, C. H. de Groot, J. Aizpurua, and O. L. Muskens, ACS Nano **6**, 6462 (2012), http://pubs.acs.org/doi/pdf/10.1021/nn3021579, URL http://pubs.acs.org/doi/abs/10.1021/nn3021579.

[28] K. Thyagarajan, S. Rivier, A. Lovera, and O. J. Martin, Opt. Express **20**, 12860 (2012), URL http://www.opticsexpress.org/abstract.cfm?URI=oe-20-12-12860.

[29] H. Aouani, M. Navarro-Cia, M. Rahmani, T. P. H. Sidiropoulos, M. Hong, R. F. Oulton, and S. A. Maier, Nano Letters **12**, 4997 (2012), http://pubs.acs.org/doi/pdf/10.1021/nl302665m, URL http://pubs.acs.org/doi/abs/10.1021/nl302665m.

[30] A. Hänsel, O. A. Egorov, S. B. Hasan, C. Rockstuhl, and F. Lederer, Phys. Rev. A **85**, 053843 (2012), URL http://link.aps.org/doi/10.1103/PhysRevA.85.053843.

[31] L. Novotny, Phys. Rev. Lett. **98**, 266802 (2007), URL http://link.aps.org/doi/10.1103/PhysRevLett.98.266802.

[32] R. Gordon, Opt. Express **17**, 18621 (2009), URL http://www.opticsexpress.org/abstract.cfm?URI=oe-17-21-18621.

[33] J. Dörfmuller, R. Vogelgesang, R. T. Weitz, C. Rockstuhl, C. Etrich, T. Pertsch, F. Lederer, and K. Kern, Nano Letters **9**, 2372 (2009), pMID: 19472987, URL http://pubs.acs.org/doi/abs/10.1021/nl900900r.

[34] S. B. Hasan, R. Filter, A. Ahmed, R. Vogelgesang, R. Gordon, C. Rockstuhl, and F. Lederer, Phys. Rev. B **84**, 195405 (2011), URL http://link.aps.org/doi/10.1103/PhysRevB.84.195405.

[35] P. B. Johnson and R. W. Christy, Phys. Rev. B **6**, 4370 (1972), URL http://link.aps.org/doi/10.1103/PhysRevB.6.4370.

[36] URL http://www.lambdaphoto.co.uk/pdfs/Inrad_datasheet_LNB.pdf.

[37] C. Hafner and J. Smajic, Journal of Modern Optics **58**, 467 (2011), http://www.tandfonline.com/doi/pdf/10.1080/09500340.2010.524317, URL http://www.tandfonline.com/doi/abs/10.1080/09500340.2010.524317.

[38] J. L. A. W. Snyder, *Optical Waveguide Theory* (Springer, 1984).

[39] A. Hayat and M. Orenstein, Opt. Lett. **32**, 2864 (2007), URL http://ol.osa.org/abstract.cfm?URI=ol-32-19-2864.

[40] R. W. Boyd, *Nonlinear Optics* (Academic Press, 2008), 3rd ed.

[41] E. Carbó-Argibay, B. Rodríguez-González, J. Pacifico, I. Pastoriza-Santos, J. Pérez-Juste, and L. M. Liz-Marzán, Angewandte Chemie **119**, 9141 (2007), ISSN 1521-3757, URL http://dx.doi.org/10.1002/ange.200703259.

[42] A. Sánchez-Iglesias, E. Carbó-Argibay, A. Glaria, B. Rodríguez-González, J. Pérez-Juste, I. Pastoriza-Santos, and L. M. Liz-Marzán, Chemistry - A European Journal **16**, 5558 (2010), ISSN 1521-3765, URL http://dx.doi.org/10.1002/chem.201000144.